Applied Energy 282 (2021) 116173

Contents lists available at ScienceDirect

Applied Energy

journal homepage: www.elsevier.com/locate/apenergy

Hydrodynamic energy harvesting analysis of two piezoelectric tandem flags under influence of upstream body's wakes

A. Mujtaba [a,1], U. Latif [a,b,1], E. Uddin [a,*], M.Y. Younis [c], M. Sajid [a], Z. Ali [a], A. Abdelkefi [d]

[a] Department of Mechanical Engineering, School of Mechanical and Manufacturing Engineering, National University of Sciences and Technology, Islamabad, Pakistan
[b] Department of Mechanical Engineering and Materials Science, Duke University, Durham, NC 27708, USA
[c] Department of Mechanical Engineering, Mirpur University of Sciences and Technology, Mirpur 10250 (AJK), Pakistan
[d] Department of Mechanical and Aerospace Engineering, New Mexico State University, Las Cruces, NM 88003, USA

HIGHLIGHTS

- Two tandem piezoelectric flags are proposed to enhance energy efficiency.
- Gap distance and velocity of the upstream body influence the energy harvesting.
- Inverted C-cylinder expands the instability region as compared to circular cylinder.
- Wakes of the upstream body increases the power output.

ARTICLE INFO

Keywords:
Piezoelectric flag
Tandem configuration
Hydrodynamic investigation
Experimental measurements
Optimal performance

ABSTRACT

In this study, the effects of the interaction of piezoelectric flags in the tandem configuration on energy harvesting in a wake flow are experimentally investigated. The flags are placed behind the bluff body and their flapping behavior is examined in terms of the flapping frequency and amplitude (peak to peak motion). The experiments are performed in a low-speed water tunnel by varying the flow velocity and streamwise gap behind an inverted C-shape cylinder to determine the influence of wake flow on the oscillating amplitude, flapping frequency, and harvested power by the piezoelectric flags. Threshold values for energy harvesting of streamwise gap and water speed are found to be the same for both flags, 1.5 and 0.18 m/s, respectively. The results show that inverted drafting is observed in flags in which the flapping amplitude of the rear flag is increased by excitation from the vortices and wake of the front flag. This interaction boosts the energy harvester efficiency based on the flapping frequency and the random excitations with high amplitudes. It is observed that as the streamwise gap in-between the flags changes, the influence of the front flag on downstream flag alters, and dynamical behavior of front flag show variation when the distance between bluff body and front flag varies. The highest power is also obtained for the rear flag at a gap of 1.75 and water speed of 0.26 m/s. The tandem configuration produces 116% more power and significantly improves the energy harvesting efficiency as compared to the single flag energy harvester.

1. Introduction

Due to the drastic change in environment and the dramatic upsurge in energy consumption in daily life, harvesting unexploited energy from the ambient fluid flow, which is available in abundance in the natural environment, and transforming it into beneficial electrical energy has been of interest for the past decade. In recent times, the focus of research has been shifted to the development of renewable and sustainable energy sources from conventional fossil fuels [1]. That is why a swift upgrade in electrical systems is seen as the development of micro-electromechanical systems (MEMS), wireless sensors for monitoring structure health [2], sensors for industrial systems, and demand for energy-efficient equipment is increasing [3]. The self-powering technologies can operate without batteries for energy storage/power source [4] and thus can easily be handled in remote locations without the tedious process of maintenance [5]. Operational costs are also reduced

* Corresponding author.
E-mail address: emaduddin@smme.nust.edu.pk (E. Uddin).
[1] Equal contribution by both leading authors.

https://doi.org/10.1016/j.apenergy.2020.116173
Received 7 August 2020; Received in revised form 28 October 2020; Accepted 30 October 2020
Available online 16 November 2020

since the replacement of batteries is no longer necessary [6].

Several types of unexploited energy exist in the ambient environment, such as solar, mechanical, acoustic, thermal, and fluid flow, and can be extracted using different transduction mechanisms like electrostatic [7], electromagnetic [8], and piezoelectric [9]. Among these, vibration and pressure driven energy harvesters are quite popular and widely studied due to their ease of application, high energy density, efficiency, and miniaturization perspective [10]. The piezoelectric transduction showed ample advantages over its counterparts and gained significant attention of researchers for harvesting energy from cantilever beams and developing small scale energy harvesters to power self-sustainable devices and sensors in inaccessible areas [9]. Energy can be harvested from the vortices produced behind a bluff body in a fluid flow [11] because vortex-induced vibration has proven to be a great source of energy extraction [12]. The rectangular plate was used as a bluff body to study the energy harvesting from wake flow and it was reported that the energy harvesting from the piezoelectric sheet is a function of flapping frequency, flapping amplitude, sheet thickness, and curvature [13]. An array of piezoelectric membranes used to study the effects of multiple membranes on energy harvesting behind a rectangular bluff body and their influence on one another while flapping [14]. These studies explored a unique way to harvest energy from flowing fluid and introduced the efficient use of wasted environmental energy which is abundantly available in our surroundings. Taylor et al. [15] reported about the available potential for power generation in flowing fluid which is equal to the cube of the flow velocity and endorsed its feasibility of extracting energy from wake flow behind a bluff body. Beal et al. [16] showed that a flexible body behind a cylinder can benefit from oncoming vortices by extracting energy from them. Placement of piezoelectric flags in the uniform flow in a specific arrangement can be advantageous for energy harvesting as studied by Lua et al. [17].

Geometric and flow parameters play a very crucial role in the performance of energy harvesters including flow speed [18], stability [19], spacing ratio [20], load resistance [21], angle [22], and shape of the bluff body [23]. Shi et al. [24] studied the influence of a low aspect ratio on the flapping behavior and distribution of strain energy at various Reynold numbers. They further investigated the effects of high aspect ratio and found that flapping amplitude increased and promoted the transition from beam like motion to wave-like motion [25]. Naturally, the flapping wing of birds in air and motion of fish with fins in water behave like a flexible structure in fluid and their motion affects the motion of other flexible structures behind it because of vortices produced from them [26]. The energy conversion is completed in two processes. Firstly, fluid's kinetic energy is converted into mechanical energy, generates strain in the flag, [27] and then the developed strain in the piezoelectric flag is converted into electrical energy [28]. Kim et al. [29] explained the dynamics of the flag in a fluid flow when placed in inverted orientation and observed different flapping modes with the conclusion that a flapping flag can produce several times higher elastic strain in comparison with a deformed flag due to the applied unsteady fluid force. In the next study, they presented the comparison of flapping for a conventional as well as inverted flag behind a solid plate and showed that conventional flag has limited tendency to flap as compared to the inverted flag [27]. They also showed that streamwise gap and velocity are key parameters for synchronization [30]. Shan et al. [31] proposed an energy harvester consists of two circular cylinders as an extension of piezoelectric substrate and the only extended portion was inserted into the water in tandem arrangement. The output efficiency was very exciting for the downstream cylinder, as a power of 167.8 μW was obtained with the freestream velocity of 0.306 m/s and the streamwise gap (L/D) of 2.5 for upstream cylinder. The downstream energy harvester showed a very optimistic results of power output of 533 μW at a streamwise gap of 1.7 and flow velocity of 0.412 m/s.

Several bluff body shapes including circular [32,33], modified circular [34,35], square, D shape [36], triangular prism, PTC cylinder [37], flat plate [30], rectangular [38], arc shape [39], T-shape [40], Y-shape [41,42] are used to expand the instability region and improve the energy harvesting efficiency. Hu et al. [35] modified the circular cylinder by attaching different cylinders of small diameters on a different angle at the circumference and recommended an angle of 60° for the optimal performance of the energy harvester. The flexible flag can be arranged in two different ways, a conventional flag configuration (in which the head of the flag is clinched and the other end is free to move) and an inverted arrangement (in which the downstream end is fixed and the head/upstream end is free to move). The conventional flag shows a completely different flapping behavior from an inverted flag. The inverted flag shows a large flapping amplitude as compared to a conventional flag at the same velocitysince the inverted flag is less stable than the conventional flag [30]. Many researchers used different configurations with the conventional [28] and inverted flags [43,44] to improve the energy harvesting performance, placing the flags in tandem [26], side by side [45], and multiple flags in diamond or conical arrangement [46]. The interaction of uniform flow with flags causes flapping and it is observed that the rear/downstream flag shows a larger amplitude when both flag flaps [47]. When placed in tandem configuration, the front flag shows a strong influence on the rear flag due to vortex generation from its tip in the wake region, and drag on upstream flag reduces [48]. The difference between the drag of the front and rear flags was explained by the vortex structures and material of flags that must be the same to hold inverted drafting phenomenon [49].

They placed the flexible flag in laminar flow and studied the influence of the upstream flag wake on downstream flags. Neither did they use upstream bluff body/cylinder for vortex shedding nor have they studied the energy harvesting in this fashion to date. The previous studies are about the dynamics and coupling of flexible flags, explaining conventional and inverted drafting phenomenon specifically. They performed numerical modelling and computational (CFD) analysis without incorporating wake instability of the bluff body. Moreover, such numerical models did not provide a realistic estimation about energy harvesting potential, lacked experimental validation, and were restricted to 2D simulations. To date, more realistic results using experiments in turbulent environment, 3-D flow, are not obtained, thus necessity to obtain energy harvesting in an environment close to the reality needs to be evaluated. This study will not only provide the results of energy extraction for tandem membrane arrangement but will also be used for validation of future 3-D computational work. So, an independent study is required to estimate the energy harvesting potential of two tandem flags influenced by the wakes of the upstream body. Therefore, it is worth investing substantial effort in this theme.

In this study, an energy harvesting system is proposed based on vortex-induced vibration (VIV) that customs two piezoelectric flags in a tandem arrangement. Flags are placed behind a unique shape of the bluff body *i.e.* inverted hollow C-shape. Both flags are placed in-line withthe center of the cylinder and the rear flag gets the advantage of improving its dynamical behavior from the wake and vortices of the front flag. The distance between the bluff body and piezoelectric flag is an important parameter to determine the response of the flag. Firstly, the streamwise gap for the front flag, Gx_1 is varied from 0.75 to 2.25 behind the bluff body to study the influence of the cylinder wakes on the front flag's energy harvesting. Gx_1 is the ratio of the distance between the center of the bluff body and the leading edge of the piezoelectric flag to the diameter of the cylinder. The position of the front flag is fixed at Gx_1 $(S1/d) = 1.75$ from the bluff body, as it turned out to be an optimal position for energy harvesting.Then the position of the rear flag is varied at the same scale and range of Gx_2 $(S2/d) = 0.75$–2.25. The Gx_2 for the rear flag is measured from the tip of the front flag. The flow velocity (U) is varied from 0.127 m/s to 0.257 m/s. The circular cylinder is used as a benchmark for a single flag harvester and additionalexperiments are conducted for performance improvement behind an inverted C-shape cylinder for tandem configuration.

2. Experimental setup and water tunnel testing

The schematic of the experimental setup is described in Fig. 1. Experiments are performed in a low-speed water tunnel with a velocity range of 0–0.5 m/s and having the test section of 2000 × 400 × 400 mm (L × W × H). The water tunnel is driven by a centrifugal pump and its RPM is controlled using a variable frequency drive (VFD) ranging from 1 to 50 Hz. So, the velocity of the water tunnel can be adjusted between 0.1 and 0.5 m/s. The piezoelectric flags (PVDF DT2-052K/L w/rivets, P/N: 2-1003744-0, Measurement Specialties Inc.,) are attached to thin steel rods, Φ = 4 mm, and the rods are clamped in a fixture over the walls of the test section.

The piezoelectric flags are placed in a conventional arrangement, clamped at leading edge and free at trailing edge, behind the cylindrical bluff body in uniform flow. The streamwise gap between flags and bluff body is adjustable through a mounting mechanism. The total length and height of flags are 74 and 16 mm, respectively, but active length is 64 mm as the terminals are waterproofed with epoxy and adhesive tape. These values are kept constant throughout this study. A circular cylinder is used as a baseline case and an inverted hollow C-shaped aluminum cylinder is used as a bluff body for tandem configuration, as shown in Fig. 1. The diameter of both cylinders is kept 25 mm to avoid blockage effect with respect to the test section. Details of the parameters used during the experimentations are described in Table 1.

A high-speed camera (Sony RX100 IV, mounted beneath the test section) is used to record the videos of flags to determine the flapping behavior at 50 frames per second for 120 s. Two flashlights are used for illumination and fixed sideways for better visualization and video recording. The remaining test section is concealed with a thick cloth to make the flag visible and prominent. A DAQ card (National Instrument, USB 6007) is used as a data acquisition system to record the voltage generated from the piezoelectric flags and both flags are connected with the same DAQ card at different input channels. Load resistance of 1MΩ is used to calculate the power output according to the maximum power transfer theorem [50]. Moreover, the output is measured against different values of the electrical load resistance and found the same value of 1MΩ, as shown in Fig. 2. Voltage data is gathered at a frequency of 50 Hz for both flags. Labview® software is used to read and save the data for further analysis and postprocessing for the same duration as videos. The image processing technique is used to determine the tail position of the flag to calculate peak to peak amplitude (A/L) and the Fast Fourier Transform (FFT) technique is implemented to find out the dominant flapping frequency using MATLAB®.

Table 1
Proposed energy harvesters' parameters.

Parameter	Value
Cylinder diameters (d)	25 mm
Cut angle of the cylinder (α)	180°
Blockage ratio	6.25%
Young's modulus (E)	1.38 GPa
Poisson's ratio (ν)	0.46
Density (ρ_f)	1.75×10^3 kg/m^3
Active length (L)	62 mm
Width (w)	12 mm
Thickness, (t)	52 μm
Load resistance (R)	1 MΩ
Generated voltage (V)	10 mV–100 V

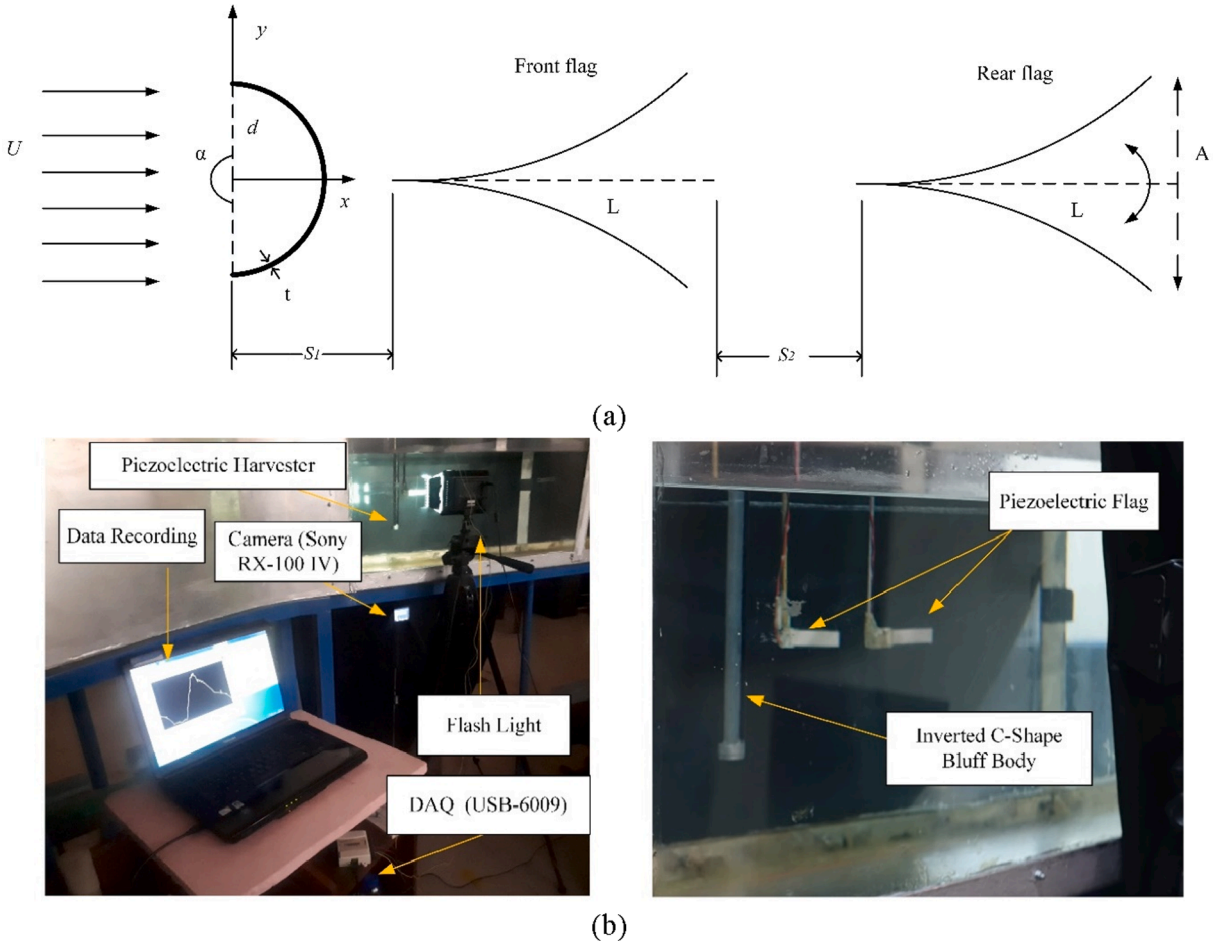

Fig. 1. (a) Schematic of the two tandem conventional flags and (b) experimental setup.

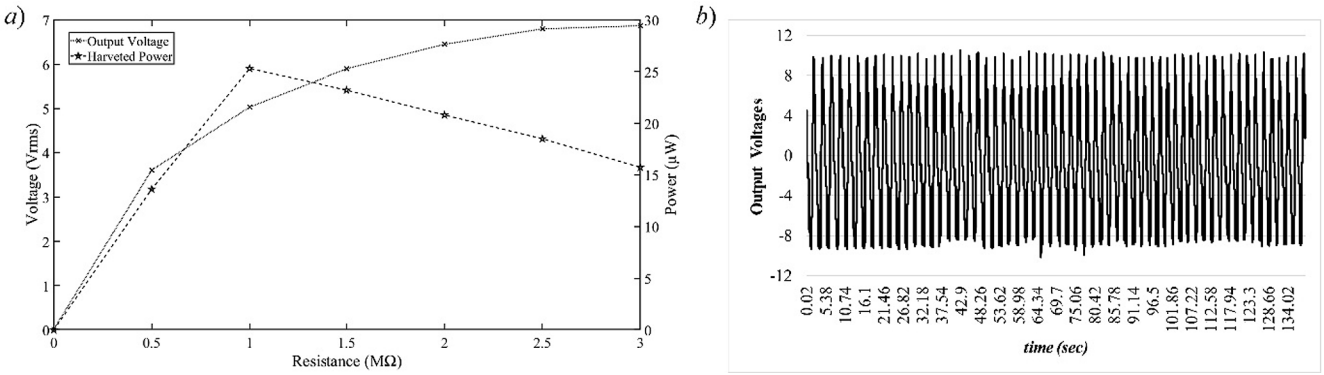

Fig. 2. (a) Output power and voltage against different load resistance and (b) temporal graph of the output voltage.

3. Results and discussion

The deformation of the piezoelectric flag and hence the levels of the harvested power depend on many factors such as water flow velocity, bending stiffness, length, thickness of flag, and fluid pressure. If both flags are compared, then the downstream flag shows a larger flapping amplitude. The difference in the flapping amplitude of the front and rear flags are explained by the wake flow of multiple flags. Vortices merge either constructively or destructively [51]. To investigate the effects of flapping dynamics and interaction of two conventional flags in the tandem arrangement in a wake flow on the energy harvesting, the streamwise gap Gx between two flags and cylinders is varied from 0.75 to 2.25. The flow velocity U is varied from 0.127 to 0.257 m/s. Below a water velocity of 0.17 m/s, the viscosity effect remained dominant so the flag does not show any significant flapping and remains in a straight mode. All the other variables are kept constant throughout this study. The position of the front flag behind the bluff body is fixed at a gap of $Gx_1 = 1.75$ because at this position the front flag shows the highest

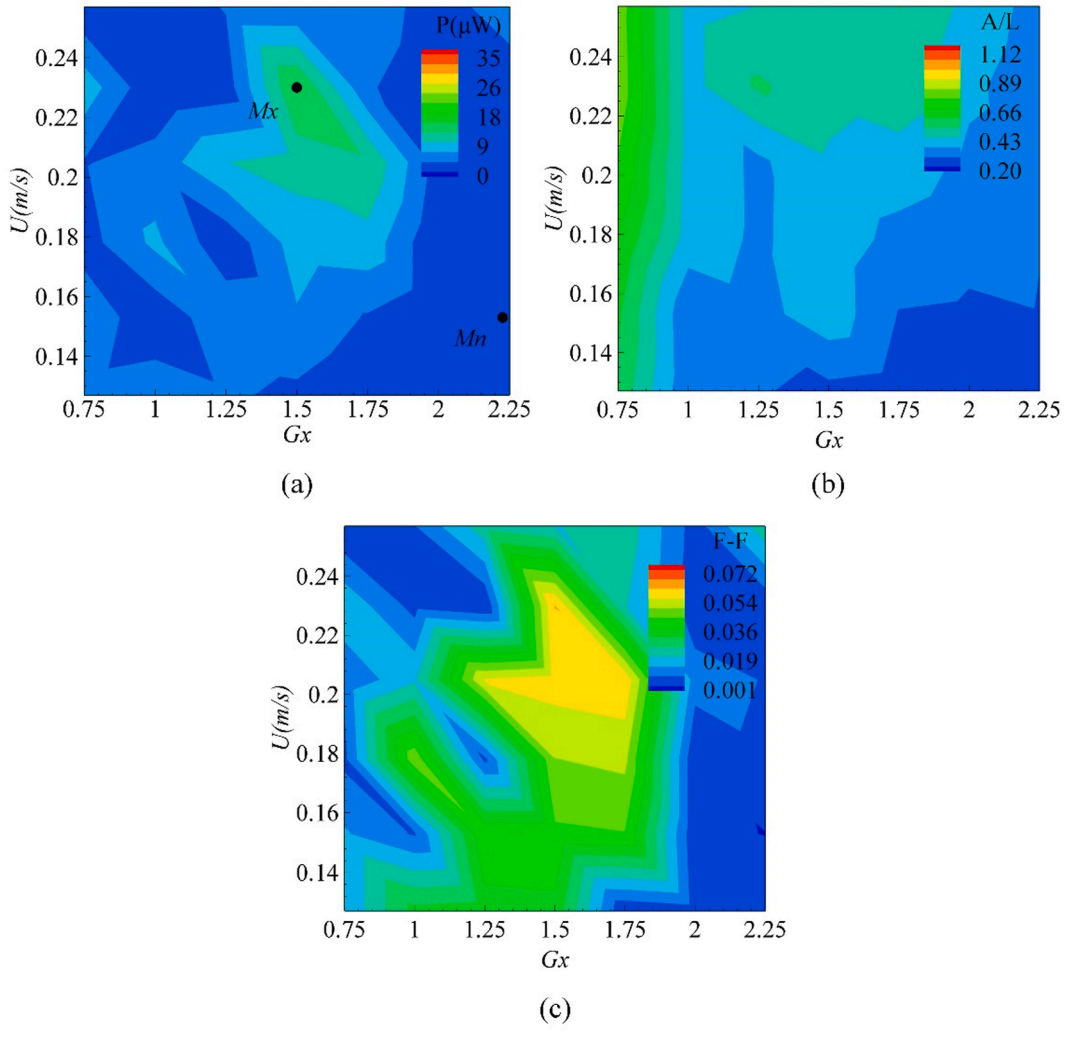

Fig. 3. (a) Harvested power, (b) peak-to-peak flapping amplitude (A/L), and (c) flapping frequency for the baseline scenario.

flapping amplitude and gives a maximum output power. The gap of the front flag is measured from the center of the cylinder to the fixed end of the flag. Concerning the rear flag, the gap is measured from the trailing edge of the front flag to the fixed end of the rear flag and both are non-dimensionalized with the cylinder's diameter.

3.1. Energy harvesting behind circular cylinder: A baseline scenario

The circular cylinder is taken as a baseline case for comparing performance improvement for flag based energy harvester. Fig. 3 shows the results of energy harvesting when a piezoelectric flag is placed behind the circular cylinder, and its output is measured as a function of the streamwise gap and fluid velocity. The maximum energy is harvested for the gap range $Gx = 1.25$–1.75 and the velocity range $U = 0.2$–0.24 m/s. The minimum energy output is observed beyond $Gx = 1.75$. To investigate this behavior, the oscillation amplitude of the piezoelectric flag (Fig. 3(b)) and flapping frequency (Fig. 3(c)) are determined and analyzed. Beyond $Gx = 1.75$, the flapping amplitude and frequency drop to the lowest value due to which the harvested energy is reduced. The highest energy found for this case is marked with point "*Mx*" ($Gx = 1.5$ at $U = 0.23$ m/s), similarly, the lowest energy point is highlighted with "*Mn*" ($Gx = 2.25$ at $U = 0.15$ m/s). The stroboscopic images of the piezoelectric flag showing the flapping trace for the peak and lowest generation points are shown in Fig. 4(a) and 4(b), respectively. The flapping flag attains a maximum amplitude (A/L) of 0.8 in the wake of a circular bluff body, which is in good agreement with the literature [52].

3.2. Output performance of front piezoelectric flag

Initially, only one flag is placed in the wake of the inverted C-shape bluff body, and analyzed for its energy harvesting performance for a range of streamwise gaps and velocities, as presented in Fig. 5(a). Likewise, its dynamical behavior in terms of flapping amplitude and frequency as a function of the velocity and streamwise gap distance Gx_1 is also investigated, as shown in Fig. 5(b) and 5(c). Fig. 5(a) marked two major regions for energy harvesting, where the first region is representing the low energy harvesting ($Gx_1 \leq 1.5$ for all flow velocities) and the second region is showing high energy output and bounded by $1.5 \leq Gx_1 \leq 2.25$. The highest energy output is obtained at $Gx_1 = 1.75$ and $U = 0.257$ m/s and the same point is marked with *Mx* in Fig. 5(a). The corresponding values of flapping amplitude and frequency are also high as depicted in Fig. 5(b) and 5(c), respectively. This shows a high strain rate which results in high energy output at point *Mx*. This can be explained with the Euler-Bernoulli beam theory which states that higher bending means higher strain energy in the beam. At low values of streamwise gap $0.75 \leq Gx_1 \leq 1.5$ and flow velocity $0.127 \leq U \leq 0.18$ m/s, the harvested levels of power remain low in this region due to the poor synchronization of wake flow with the flag and does not produce any significant motion/flapping in the piezoelectric flag, as indicated in Fig. 6(b). Even for the higher value of Gx_1, a minor growth in energy output is observed at $0.127 \leq U \leq 0.18$ m/s due to the viscous effect of water so vortex shedding and unsteady forces dampen or weak as it approaches the piezoelectric flag, resulting in low corresponding flapping amplitude and frequency. Hence, low energy transfer from wake flow to piezo-flag happens as shown in Fig. 5 and marked with point *Mn* ($Gx_1 = 1.25$ and $U = 0.127$ m/s).

Another but narrow region of low energy is observed *i.e.* $0.75 \leq Gx_1 \leq 2.25$ for a low flow velocity range. By disentangling this region from the rest of the graph and comparing it with its dynamical behavior, it reveals that the vortical structure or free shear layer in the wake does not interact properly with the piezoelectric flag, so the poor extraction of energy is observed for this region too and most of the flow energy gets wasted. By making a further increase in the $Gx_1 > 1.5$ and $U > 0.18$ m/s, a high energy region is observed. Furthermore, inspecting the plots in Fig. 5(b) and 5(c), the minimum flapping frequency of 0.003 and minimum flapping amplitude (A/L) of 0.31 are experimentally obtained.

It should be mentioned that the flag behind the inverted C-shape cylinder yields 102.80% higher energy output compared to the circular cylinder, as indicated in Fig. 3(a) and 5(a). It is demonstrated in this experiment that, in a conventional flag, as the flow velocity increases, the flapping amplitude of the flag increases until it goes from periodic flapping to erratic flapping mode.

3.3. Output performance of rear piezoelectric flag in a tandem configuration

After determining the optimal location and corresponding water velocity of the front flag, an investigation on the performance of the rear piezoelectric flag energy harvester and the optimal water speed and gap is performed. The rear flag is placed downstream to the front flag and inline to the cylinder axis and front flag, hence the rear flag is under influence of combined wake of inverted hollow C-shape bluff body and front flag, as shown in Fig. 1. This arrangement is the main motivation for this study. Energy harvesting performance as a function of streamwise gap Gx_2 and water velocity U and its dynamical behavior in terms of flapping amplitude and frequency are examined, as shown in Fig. 7(a-c), respectively. Fig. 7(a) shows the power output obtained for the rear flag and the plot is divided into four regions to explain the energy output trend/behavior and regions are marked with I, II, III, and IV. Region-I shows low energy harvesting and poor synchronization of wake flow

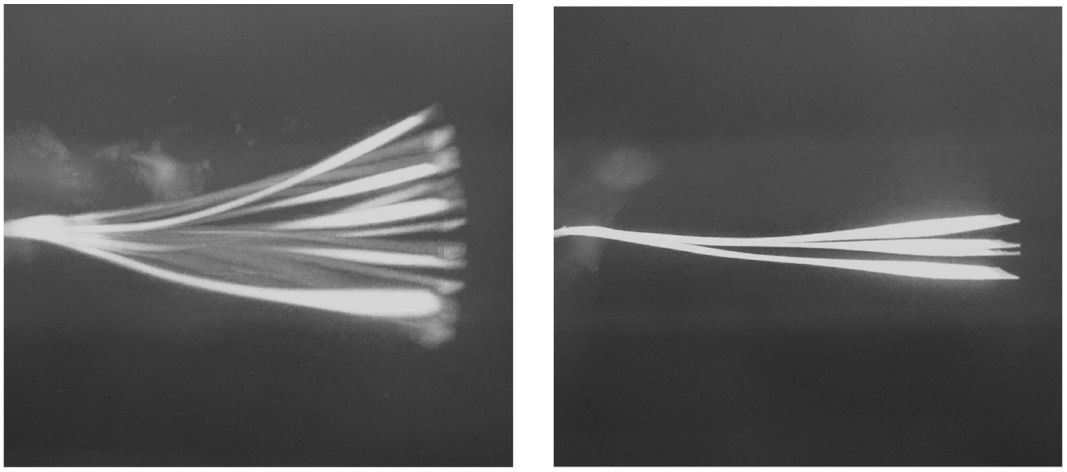

Fig. 4. Stroboscopic images of flag energy harvester at (a) $Gx = 1.5$ and $U = 0.23$ m/s and (b) $Gx = 2.25$ and $U = 0.153$ m/s.

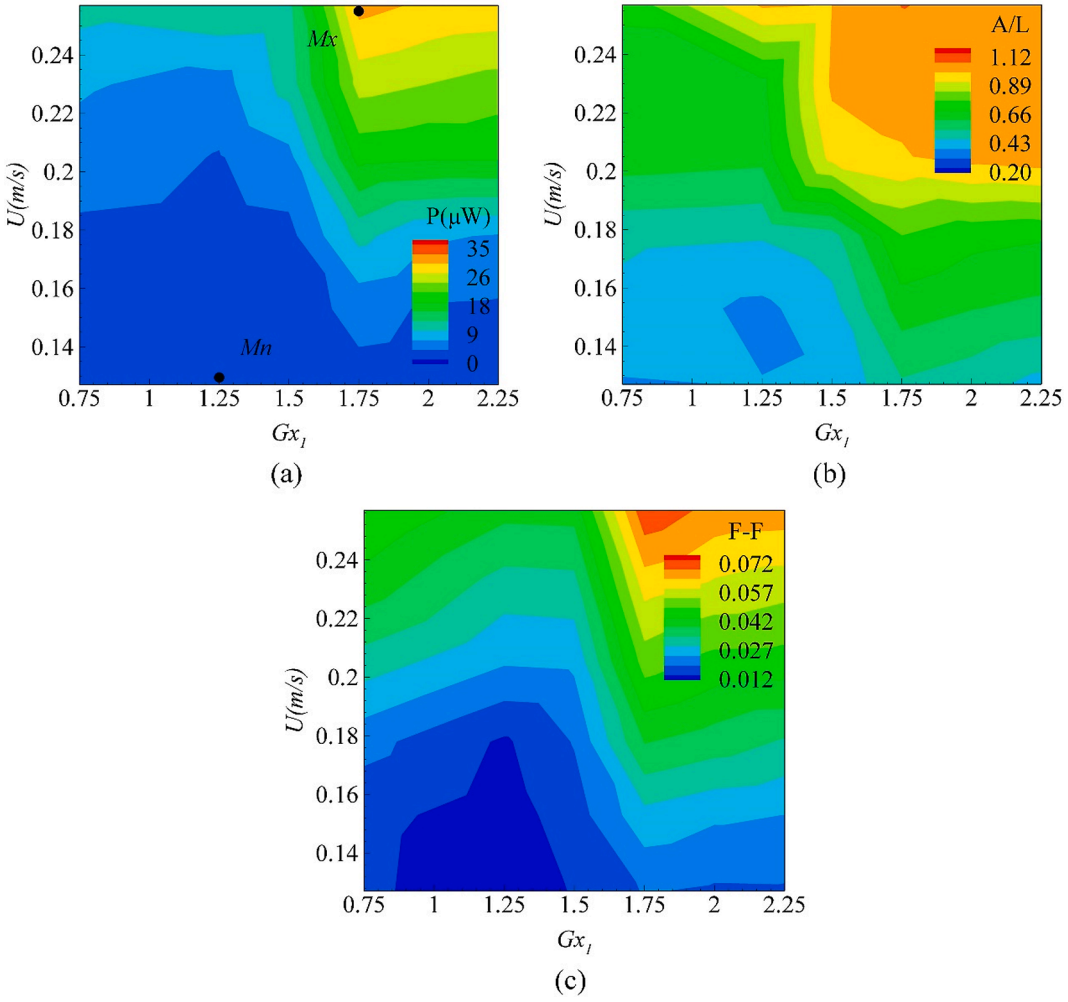

Fig. 5. (a) Output power, (b) peak-to-peak amplitude (A/L), and (c) flapping frequency for a single flag energy harvester.

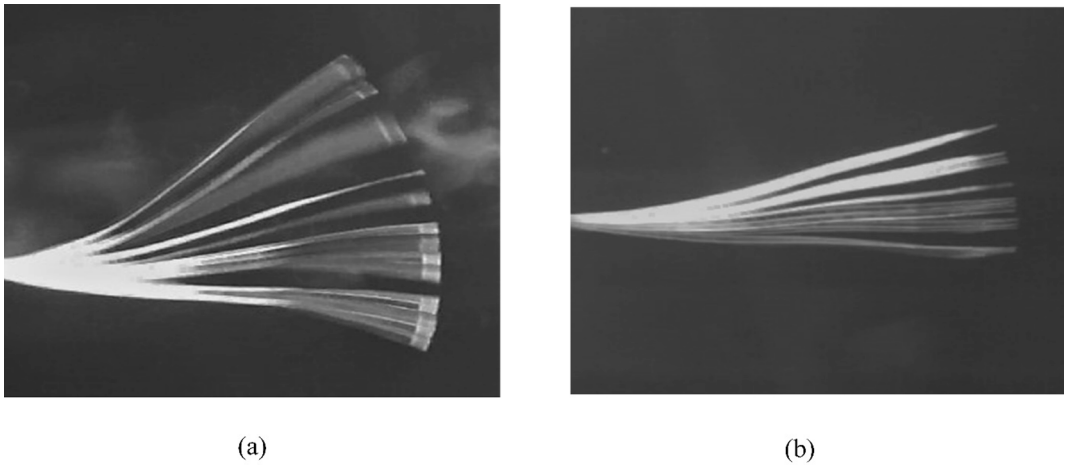

Fig. 6. Stroboscopic images of flag energy harvester at (a) $Gx_1 = 1.75$ and $U = 0.257$ m/s and (b) $Gx_1 = 1.25$ and $U = 0.127$ m/s.

with the rear flag, whereas regions II & III indicate transition from low to high power and pre-synchronization of wake flow with the rear flag. Region-IV presents the higher output of electrical power which is attributed to the optimal coupling of wake flow with the flag.

The point, where the highest energy output is obtained marked with *Mx* in Fig. 7(a), represents a maximum energy generation at $Gx_2 = 1.75$ and $U = 0.257$ m/s and the corresponding points on Fig. 7(b) and 7(c) represent the maximum flapping amplitude and flapping frequency. This shows a high deformation in the rear flag, analogous to bending energy, which results in high generated voltage at point *Mx*. When the flow velocity is becoming higher than 0.16 m/s, the vortex shedding from the cylinder becomes stronger. By increasing the water velocity, the size of the vortex decreases but the number of shed vortices from the upstream body increases [53], due to which output power, flapping

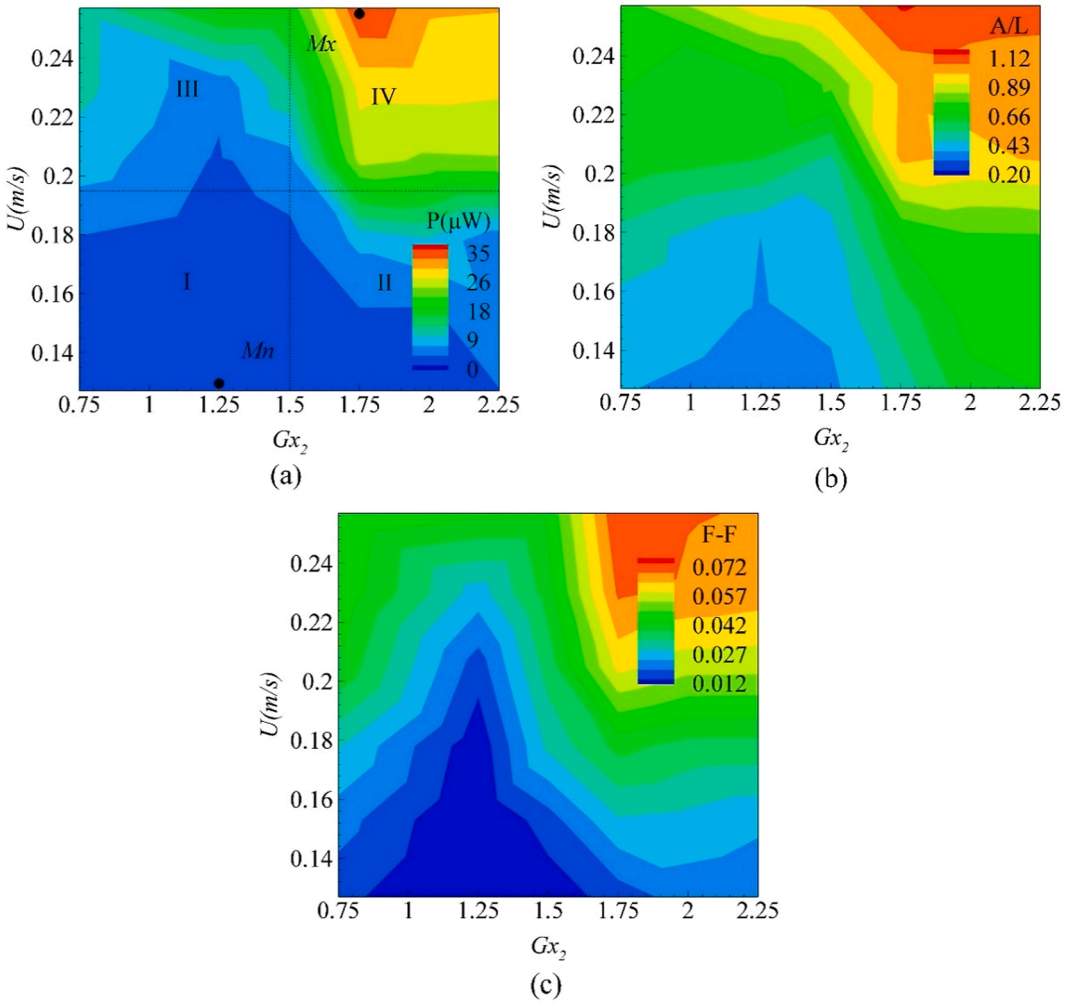

Fig. 7. (a) Output power, (b) peak-to-peak amplitude (A/L), and (c) flapping frequency for the rear flag energy harvester performance.

amplitude, and frequency start to increase prominently and specifically at a higher value of $Gx_2 \geq 1.5$. The regions in Fig. 7(b) and 7(c) corresponding to region-I ($Gx_2 = 0.75$–1.5 and $U = 0.127$–0.196 m/s) explain the dynamical behavior of piezoelectric flag and the reason behind low energy output as low amplitude and frequency is observed for this region which defines low strain rate. The communication between flags, modulation effect, through wakes diminished at low frequency due to soft and flexible rear flag [26], so the influence of the front flag on the rear flag gets reduced.

The minimum energy harvesting point is also identified in this region and marked with *Mn* ($Gx_2 = 1.25$, $U = 0.127$ m/s) which shows destructive interaction of rear flag with the wakes of front flag, resulting in a significant decrease in energy harvesting. For optimal results, the interaction of wakes of the front flag with the rear flag must be in a constructive manner [54] and it can be achieved by fine-tuning the relative position of the incoming vortices and fixed end of the rear flag [55]. Further increase in the flow velocity and streamwise gap causes the transition from low energy region to high energy output and marked with II & III. Fig. 7(b) and (c) verify the pre-synchronization of wake flow oscillations with the flag oscillation and show significant improvement in resulting output as compared to the region I. Further analysis of Fig. 7(a) shows that region IV ($Gx_2 = 1.5$–2.25 and $U = 0.2$–0.26 m/s) is a high energy region, where the rear flag is fully getting influenced by the coherent wake of the upstream flag and exhibits the optimal coupling of wake flow and flag oscillation. The corresponding areas of Fig. 7(b) and (c) show linkages of wake oscillation with flag oscillation which generates synchronization condition, resulting in higher harvested power output. Fig. 7(a) shows the temporal graph of tip motion of the piezoelectric flag and Fig. 7(b) depicts its flapping trace made by stroboscopic images when the rear flag is positioned at *Mx* ($Gx_2 = 1.75$ and $U = 0.26$ m/s). Likewise, Fig. 8 shows data for minimum point *Mn* ($Gx_2 = 1.25$ and $U = 0.127$ m/s). Clearly, the rear flag energy harvester has high oscillating amplitudes, as shown in Fig. 8(b) and hence it generates 16.1% higher output power in comparison to the front flag.

3.4. Combined analysis of two tandem energy harvester

3.4.1. Energy harvesting analysis of two tandem configuration

After separately studying the performance of each piezoelectric flag energy harvester, an experimental investigation on the tandem energy harvesting systems performance is carried out. Fig. 9 shows the combined power output for tandem flags behind an inverted hollow C-shape cylinder. The maximum combined power of 65.3 μW is obtained at $Gx = 1.75$ and $U = 0.257$ m/s and marked with *Mx* in Fig. 9 (for optimal power output case shows the visualization results of both upstream and downstream flags as well). Likewise, the minimum power of 0.2 μW is obtained at *Mn* ($Gx = 1.25$ and $U = 0.127$ m/s). The harvested power is calculated using $P = V^2_{rms}/R$. The optimal power is found out through matching impedance using the maximum power transfer theorem which states that for optimal resistance, the impedance of the system must be known [50]. The highest power is obtained at high water velocity $U >$ 0.18 m/s and gap $Gx > 1.5$ and the low power region is bounded in $0.127 \leq U \leq 0.18$ m/s and $0.75 \leq Gx \leq 1.5$. An increase of 116% in

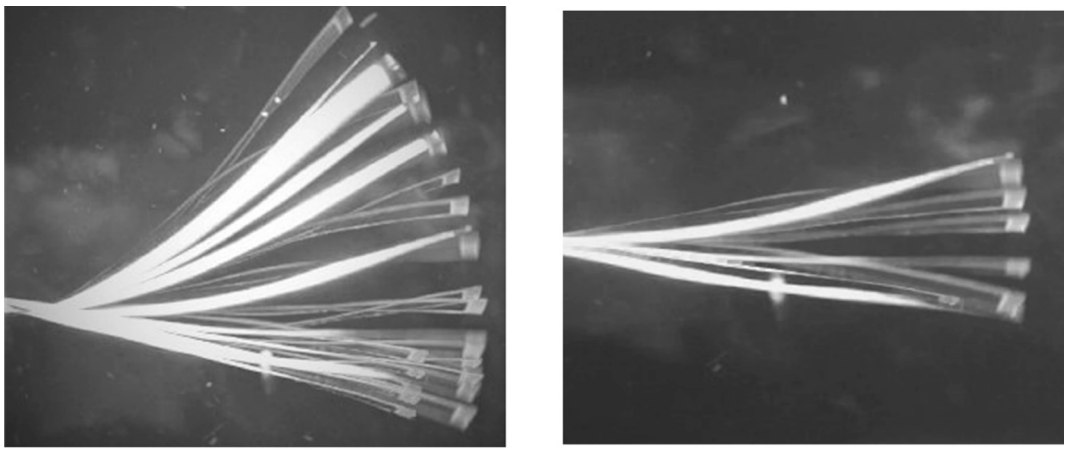

Fig. 8. Stroboscopic images of flag energy harvester at (a) $Gx_2 = 1.75$ and $U = 0.257$ m/s and (b) $Gx_2 = 1.25$ and $U = 0.127$ m/s.

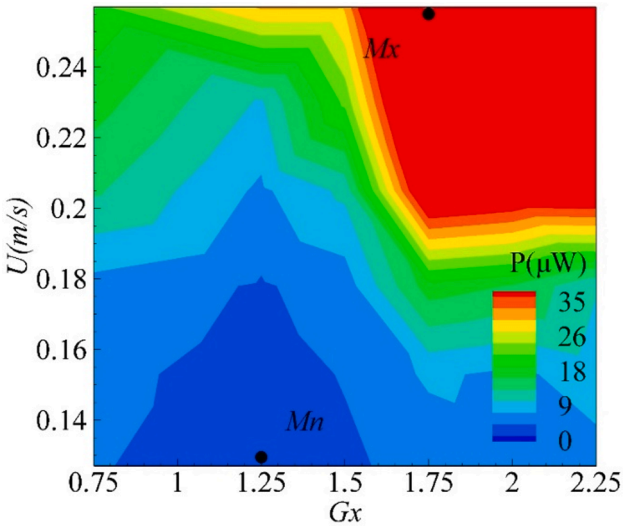

Fig. 9. Plot for the combined output power of tandem piezoelectric energy harvesting flags.

output power is observed using tandem configuration as compared to a single flag behind an inverted hollow C-shape cylinder.

There are several sensors which require only a few micro-watts of energy for their operation and the harvested energy is enough to operate them efficiently like wireless sensor node for monitoring structural and human health [56], cardiac pacemaker, and quartz watch [57]. The harvested energy can also be increased easily by using multiple piezoelectric membranes in combination [58] and optimizing the circuit [59]. Table 2 also shows the power required for their function.

Table 2
Power required for various sensors and devices.

No	Name of sensor/equipment	Required power	Reference
1	Analog-to-digital converter (ADC)	0.18–0.85 μW	[58]
2	Quartz watch	5 μW	[57]
3	STLM20 temperature sensor	12 μW	[60]
4	TSYS02P, temperature sensor	3.3 VDC	[52]
5	Cardiac pacemaker	50 μW	[57]
6	Wireless sensor node	100 μW	[57]
7	UWB transmitter IC	0.65 mW	[61]
8	Hearing aid	1 mW	[57]

Fig. 10 shows the response of the proposed energy harvesting system, two tandem piezoelectric flags behind an inverted C-shape bluff body, at different streamwise gaps Gx. The streamwise gap plays a key role in achieving systems optimal response at which maximum energy output is obtained for both flags *i.e.* $Gx = 1.75$. At the low spacing distance at $Gx_1 = Gx_2 = 0.75$, the combined system shows poor performance, hence yields low output power, as shown in Fig. 10. Further increase in the gap does not show any gain except for high velocity. It is interesting to note that at the same gap $Gx_1 = Gx_2 = 1.25$, the rear flag surprisingly shows anomalous behavior. The front flag shows a substantial gain in output voltage but the rear flag shows a significant change which indicates that the gap for the rear flag is not appropriate for proper coupling with wake flow of the upstream body and it is interacting destructively resulting in a drop in the output power for the rear flag. When the gap is increased from 1.25 to 1.50, the system shows an affirmative response for both flags and sharp gain for the rear flag specifically at $U = 0.23$ m/s. Further increase in the gap provides the optimal point in the wake for both the flags where the system is fully synchronized with the oncoming vortices from the upstream body which results in high strain rate and thus energy harvesting. So, the optimal streamwise gap for the front and rear flag is found to be $Gx_2 = 1.75$. After this, the system starts to lose its connectivity with wakes and a gradual drop in energy output is observed with further increase in streamwise gap.

Next, a particular investigation is paid on the impacts of the flow velocity on the tandem system's performance. Experiments are performed for a range of flow velocity, $U = 0.127$–0.257 m/s, and velocity is increased gradually to monitor its impact on the system's behavior, as shown in Fig. 11. Initially, with increments in the velocity, the tandem system shows a progressive increase in the levels of the harvested power for both flags. When the velocity is increased to 0.205 m/s, a sharp increase in the harvested power is observed which shows the system's response to flow velocity and can be stated as a cut in speed for optimal coupling. This sharpness is particularly observed for the rear flag energy harvester. Further increase in the water velocity causes improvement in energy harvesting and the system attains the highest value at maximum flow velocity $U = 0.257$ m/s. A noteworthy finding is that although the output power shows a linear relationship with the flow velocity for a specific range, the system shows spontaneous and instant increase in output for $U \geq 0.2$ m/s. This indicates how the front and rear flag are responding to the wakes of the upstream body as an inverted C-shape cylinder is an upstream body for the front flag whereas the front flag acts as an upstream bluff body for the rear flag. Synchronization of both flags is purely dependent on the spacing distance between the two flags and when it occurs both flags show linear response to flow velocities like F5

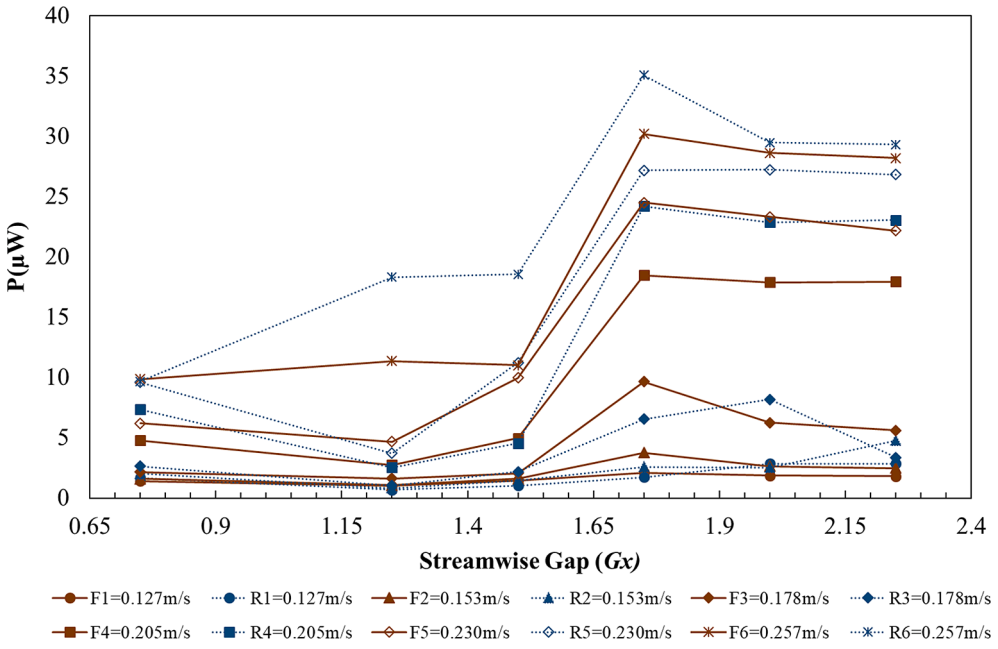

Fig. 10. Energy harvesting at different streamwise gaps (Gx = 0.75–2.25) for the two flag-based energy harvesters. "F" means the front flag and "R" means the rear flag.

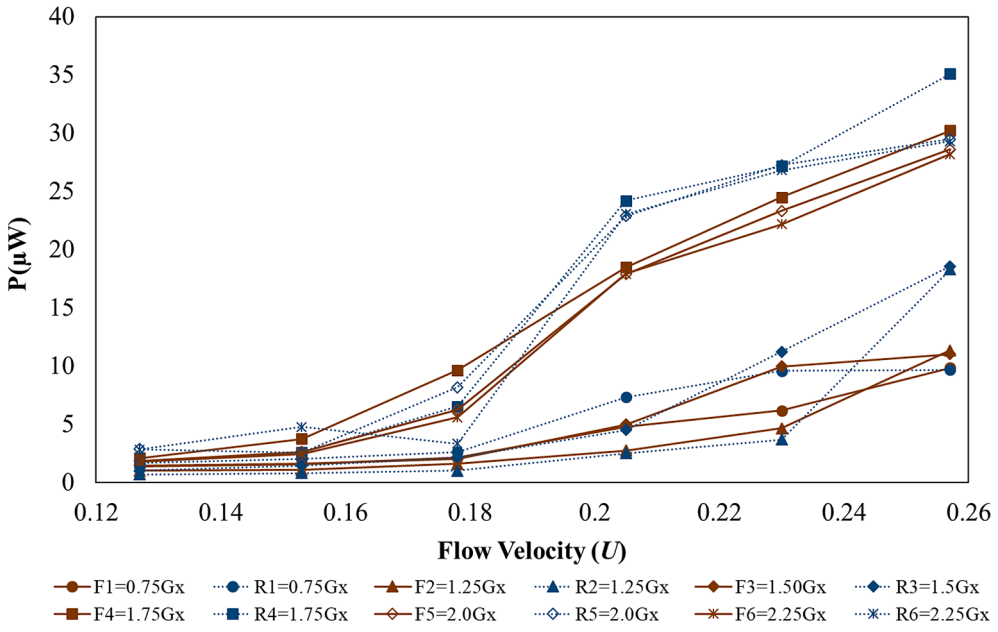

Fig. 11. Energy harvesting at different flow velocities (U = 0.127–0.257 m/s) for the two flag-based energy harvesters. "F" means the front flag and "R" means the rear flag.

and R5 but when the gap between them is not appropriate to properly link up the oscillation of a flag with oncoming vortices its response becomes erratic like F3 and R3.

3.4.2. Comparison of the dynamical behavior of two tandem energy harvesters

After deeply inspecting the optimal levels of the harvested power of the tandem energy harvesters, an experimental investigation on the influences of the spacing distances and water velocity on the dynamics of the systems as well as the oscillating frequency is performed. Fig. 12 depicts the oscillation amplitude variation of both flag-based energy harvesters with respect to the streamwise gap Gx when distinct values of the water speed are considered. It is observed that the streamwise gap has a great impact on the flapping amplitude of both piezoelectric flags. Inspecting the plotted curves in Fig. 12, it is clear that the flapping amplitudes of the two flag systems are greatly changed especially for the rear flag. To be more specific, it is noted that when the streamwise gap is small, the poor coupling of both flags with the wake flow occurred except F6 and R6 at $Gx = 1.25$. Further increase in the gap from 1.25 to 1.5 shows both kinds of interactions of flags with the flow. At $Gx = 1.5$, R4 shows a sharp decline which reflects destructive interaction of front flag wakes with rear flag whereas at the same gap front flag shows constructive interaction with the cylinder wakes and results in higher vibration amplitude. This observation explains the importance of a

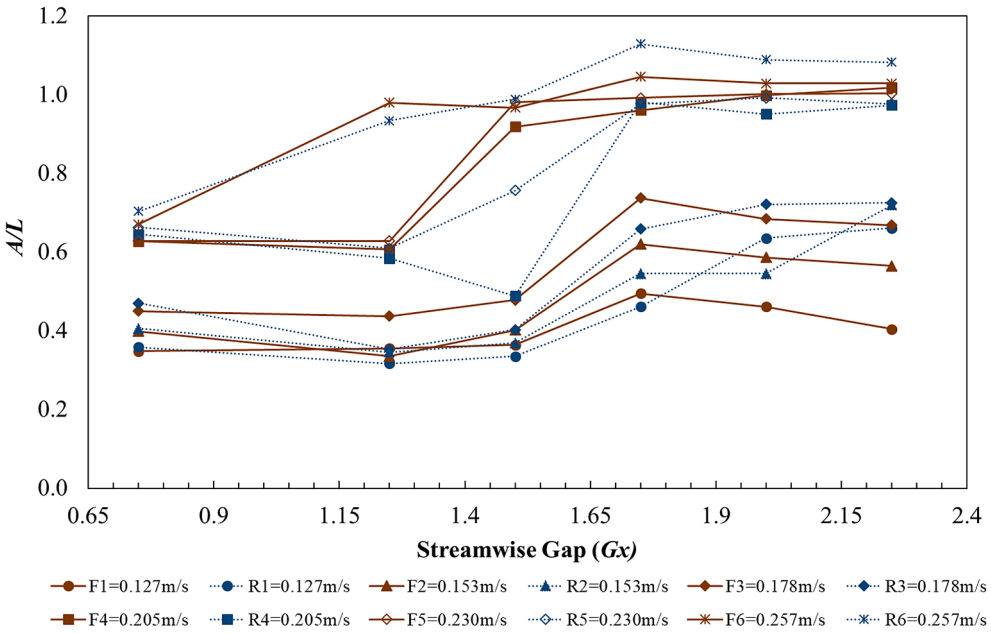

Fig. 12. Flapping amplitudes of the two flag-based energy harvesters at different streamwise gaps (Gx = 0.75–2.25). "F" means the front flag and "R" means the rear flag.

streamwise gap between the cylinder and front flag, likewise for the front and rear flag. The proposed system shows optimal coupling at Gx = 1.75 and after that, the coupled system does not show any further gain in oscillation amplitude and starts decreasing gradually with an increase in the value of Gx. Consequently, for optimal energy harvesting from the proposed combined system, Gx = 1.75 is the appropriate value of the streamwise gap to place both flags in the wake region.

In Fig. 12, the impacts of the streamwise gap for various water velocities are examined for the front and rear flag-based energy harvesting systems. The flapping frequency and synchronization remain weak till Gx = 1.5 but with the further increase in streamwise gap, the system attains optimal coupling for both flags at Gx = 1.75. After that, a gradual decrease in the flapping frequency is observed for both flags and the pattern remained the same for both flags, as shown in Fig. 13. The value of flapping frequency for R6 follows the same trend as for R5 but with a higher value. The noteworthy thing here is that for a lower value of Gx, the front flag influences the rear flag but in a destructive manner so a drop in flapping frequency is observed specifically Gx = 1.25. Increasing more Gx causes proper synchronization and the front flag influenced the rear flag in a constructive manner for all values of Gx.

To study the effects of the water speed on the tandem system's performance, Fig. 14 shows the variations of the flapping amplitudes of the two flag-based energy harvesters with respect to the water velocity. To elaborate on the oscillation amplitude of two tandem flags, the graph in Fig. 14 can be divided into two parts, namely, $0.12 \leq U \leq 0.18$ and $0.18 \leq U \leq 0.26$. Initially, the coupled system does not show any

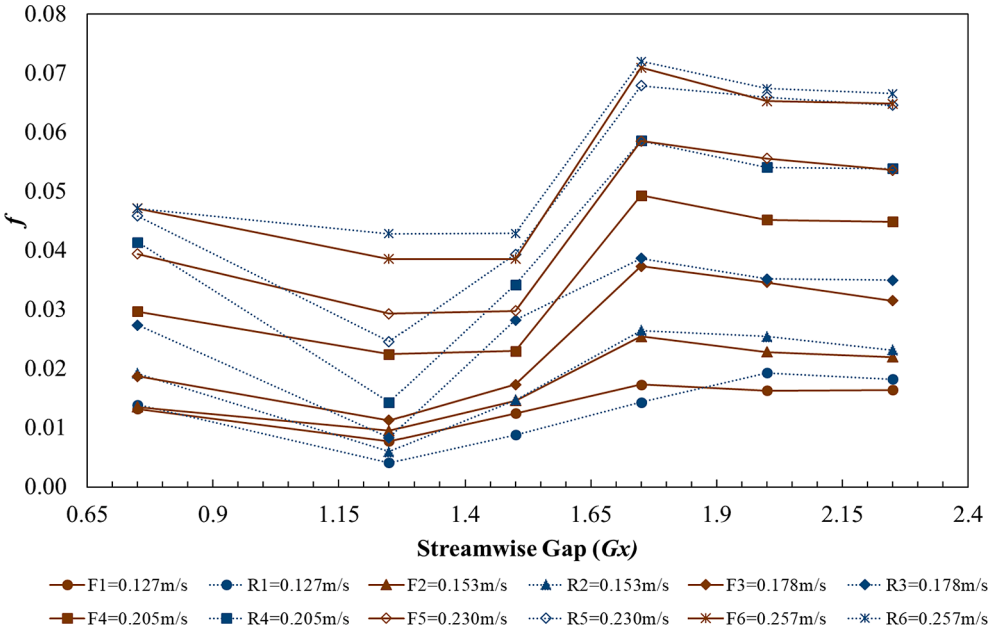

Fig. 13. Dominant oscillating frequency for both flag-based energy harvesters at different streamwise gaps (Gx = 0.75–2.25). "F" means the front flag and "R" means the rear flag.

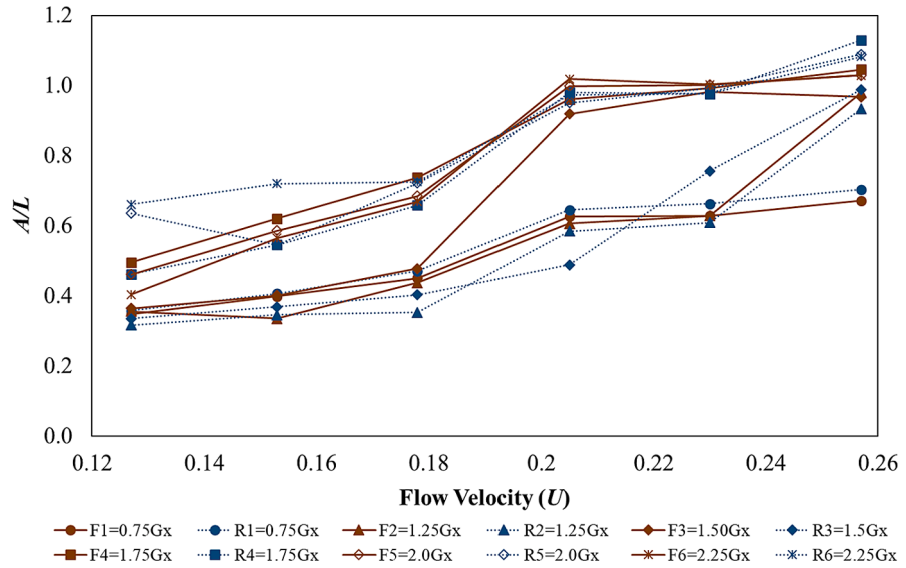

Fig. 14. Flapping amplitudes of the two flag-based energy harvesters at different flow velocities ($U = 0.127$–0.257 m/s). "F" means the front flag and "R" means the rear flag.

considerable gain in oscillation amplitude for $U \leq 0.18$. With further increase in the flow velocity, both flags show constructive interaction with the wakes. The contradictory behavior of F3 and R3 explains the influence of the front flag on the rear flag amplitude, as the front flag is placed at $Gx = 1.5$ from the cylinder. Clearly, the coupling with wake flow takes place but when the rear flag is placed at $Gx = 1.5$ from the front flag, no influence on the rear flag is observed resultantly poor oscillation in comparison with the front flag energy harvesting system. Overall, increasing the flow velocity causes an increase in the flapping amplitudes of both flags.

Fig. 15 shows the linear impact of the flow velocity on the flapping frequency of both flags which means increasing the flow velocity, also increases the flapping frequency. The rear flag shows the distinction in the flapping frequency as compared to the front flag energy harvester and remains high for all values of flow velocities except R2 ($Gx = 1.25$). The highest flapping frequency is observed for the R4 ($Gx = 1.75$). Other than R4, the value of the flapping frequency also remains high for R5 and R6 which shows the superiority of the rear flag over the front flag. Therefore, it would be advantageous to use a tandem flag configuration for a greater power production.

4. Conclusions

In this experimental study, the energy harvesting performance of two tandem conventional piezoelectric flags in the wake of an inverted C-shape bluff body was investigated. Both energy harvesting flags convert mechanical strain energy into electrical energy. Experiments were performed by varying the streamwise gap distance Gx between the bluff body and upstream flag and then in between the flags in the tandem configuration from 0.75 to 2.25. The flapping amplitude and harvested power increased for $Gx = 1.5$–2.25 and $U \geq 0.18$ m/s. It was found that for smaller $Gx_2 \leq 1.5$ the flapping amplitude of the rear flag is reduced

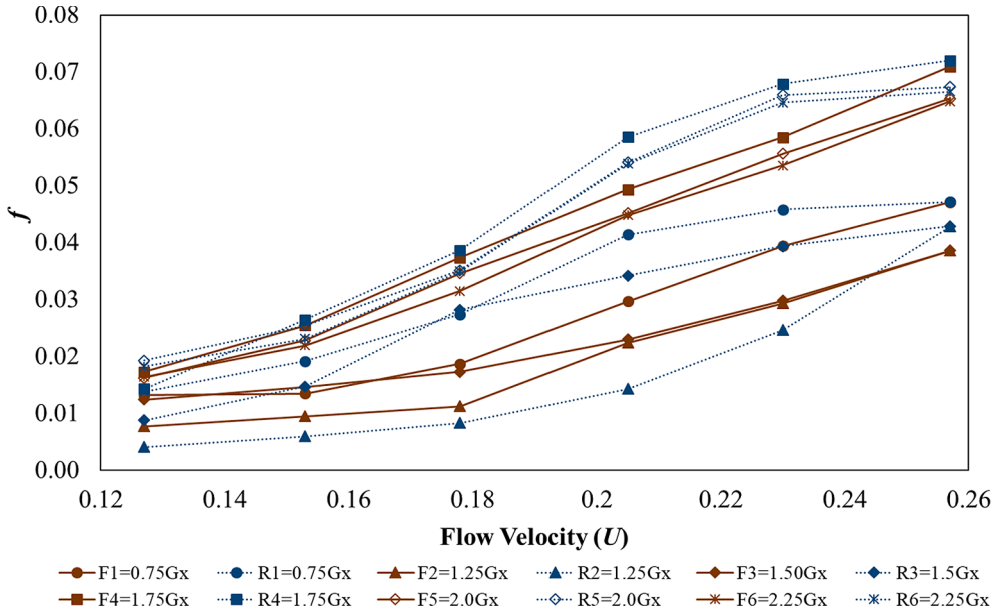

Fig. 15. Dominant frequency of the two flag-based energy harvesters at different flow velocities ($U = 0.127$–0.257 m/s). "F" means the front flag and "R" means the rear flag.

due to the destructive interaction of the tandem flags. It was also identified that the downstream flag shows the larger flapping amplitude and output power for $Gx_2 = 1.75$ and $U = 0.257$ m/s. This was caused by the constructive interaction merging mode between vortices at these separation distances, which increasethe flapping amplitude and frequency, and consequently the energy harvesting characteristics.

The threshold value of flow velocity was found to be 0.18 m/s for energy harvesting and beyond this value, the coupled system started to show synchronization with the wake flow as both flags are under the influence of wakes. Similarly, the threshold value for streamwise gap Gx is found to be 1.5, and beyond this, the system showed optimal coupling particularly at $Gx = 1.75$ and $U = 0.257$ m/s. Like wise, the rear flag also showed dependence on the streamwise gap and flow velocity for energy harvesting. For optimal coupling of the rear flag with the upstream coherent wakes, the flag should be placed at an appropriate spacing so that the synchronization condition could be achieved for optimal energy harvesting. The inverted hollow C-shape bluff body also expanded the instability region that resulted in improved wake dynamics and caused performance improvements of the proposed energy harvester. The front flag generated 30 micro-watt power and the rear flag generated 16.1% higher energy output in comparison with the front flag. Overall, the combined effect of tandem flags remained impressive and an outstanding increase of 116% is obtained in output power as compared to a single flag, which is a significant increase in energy harvesting by using a tandem configuration as compared to a single flag behind an upstream bluff body. The proposed energy harvester is simple and easy to implement as it does not require any modification in the bluff body.

CRediT authorship contribution statement

A. Mujtaba: Conceptualization, Data curation. **U. Latif:** Conceptualization, Data curation, Writing - original draft, Investigation, Visualization. **E. Uddin:** Supervision, Funding acquisition. **M.Y. Younis:** Investigation, Visualization. **M. Sajid:** Writing - review & editing. **Z. Ali:** Validation, Writing - review & editing. **A. Abdelkefi:** Writing - review & editing, Investigation.

Declaration of Competing Interest

The authors declare that they have no known competing financial interests or personal relationships that could have appeared to influence the work reported in this paper.

Acknowledgements

This research was supported by the National Research Program for Universities (NRPU) Grant 20-4794 by Higher Education Commission of Pakistan.

References

[1] Karim M, Munir A, Karim M, Muhammad-Sukki F, Abu-Bakar S, Sellami N, et al. Energy revolution for our common future: an evaluation of the emerging international renewable energy law. Energies 2018;11:1769. https://doi.org/10.3390/en11071769.
[2] Iqbal M, Khan FU. Hybrid vibration and wind energy harvesting using combined piezoelectric and electromagnetic conversion for bridge health monitoring applications. Energy Convers Manag 2018;172:611–8. https://doi.org/10.1016/j.enconman.2018.07.044.
[3] Mitcheson PD, Yeatman EM, Rao GK, Holmes AS, Green TC. Energy harvesting from human and machine motion for wireless electronic devices. Proc IEEE 2008;96:1457–86. https://doi.org/10.1109/JPROC.2008.927494.
[4] Ottman GK, Hofmann HF, Bhatt AC, Lesieutre GA. Adaptive piezoelectric energy harvesting circuit for wireless remote power supply. IEEE Trans Power Electron 2002;17:669–76. https://doi.org/10.1109/TPEL.2002.802194.
[5] Priya S. Advances in energy harvesting using low profile piezoelectric transducers. J Electroceram 2007;19:165–82. https://doi.org/10.1007/s10832-007-9043-4.
[6] Sudevalayam S, Kulkarni P. Energy harvesting sensor nodes: Survey and implications. IEEE Commun Surv Tutorials 2011;13:443–61. https://doi.org/10.1109/SURV.2011.060710.00094.
[7] Hammad B, Abdelmoula H, Abdel-Rahman E, Abdelkefi A. Nonlinear analysis and performance of electret-based microcantilever energy harvesters. Energies 2019;12:4249.
[8] Beeby SP, Torah RN, Tudor MJ, Glynne-Jones P, O'Donnell T, Saha CR, et al. A micro electromagnetic generator for vibration energy harvesting. J Micromech Microeng 2007;17:1257–65. https://doi.org/10.1088/0960-1317/17/7/007.
[9] Abdelkefi A. Aeroelastic energy harvesting: A review. Int J Eng Sci 2016;100:112–35.
[10] Maamer B, Boughamoura A, Fath El-Bab AMR, Francis LA, Tounsi F. A review on design improvements and techniques for mechanical energy harvesting using piezoelectric and electromagnetic schemes. Energy Convers Manag 2019;199. https://doi.org/10.1016/j.enconman.2019.111973.
[11] Hu Y, Yang B, Chen X, Wang X, Liu J. Modeling and experimental study of a piezoelectric energy harvester from vortex shedding-induced vibration. Energy Convers Manag 2018;162:145–58. https://doi.org/10.1016/j.enconman.2018.02.026.
[12] Naseer R, Dai H, Abdelkefi A, Wang L. Piezomagnetoelastic energy harvesting from vortex-induced vibrations using monostable characteristics. Appl Energy 2017;203:142–53.
[13] Allen JJ, Smits AJ. Energy harvesting EEL. J Fluids Struct 2001;15:629–40. https://doi.org/10.1006/jfls.2000.0355.
[14] Techet AH, Allen JJ, Smits AJ. Piezoelectric EELS for energy harvesting in the ocean. Proc Twelfth Int Polar Eng Conf 2002;3:713–8.
[15] Taylor GW, Burns JR, Kammann SM, Powers WB, Welsh TR. The energy harvesting Eel: A small subsurface ocean/river power generator. IEEE J Ocean Eng 2001;26:539–47. https://doi.org/10.1109/48.972090.
[16] Beal DN, Hover FS, Triantafyllou MS, Liao JC, Lauder GV. Passive propulsion in vortex wakes. J Fluid Mech 2006;549:385–402. https://doi.org/10.1017/S0022112005007925.
[17] Lua KB, Lu H, Zhang XH, Lim TT, Yeo KS. Aerodynamics of two-dimensional flapping wings in tandem configuration. Phys Fluids 2016;28.. https://doi.org/10.1063/1.4971859.
[18] Deivasigamani A, McCarthy JM, John S, Watkins S, Trivailo P, Coman F. Flutter of cantilevered interconnected beams with variable hinge positions. J Fluids Struct 2013;38:223–37. https://doi.org/10.1016/j.jfluidstructs.2012.10.011.
[19] Wang J, Geng L, Zhou S, Zhang Z, Lai Z, Yurchenko D. Design, modeling and experiments of broadband tristable galloping piezoelectric energy harvester. Acta Mech Sin Xuebao 2020. https://doi.org/10.1007/s10409-020-00928-5.
[20] Usman M, Hanif A, Kim IH, Jung HJ. Experimental validation of a novel piezoelectric energy harvesting system employing wake galloping phenomenon for a broad wind spectrum. Energy 2018;153:882–9. https://doi.org/10.1016/j.energy.2018.04.109.
[21] Dai H, Abdelkefi A, Wang L. Piezoelectric energy harvesting from concurrent vortex-induced vibrations and base excitations. Nonlinear Dynamics 2014;77:967–81.
[22] Abdelkefi A, Hajj M, Nayfeh A. Piezoelectric energy harvesting from transverse galloping of bluff bodies. Smart Mater Struct 2012;22:015014.
[23] Latif U, Uddin E, Abdullah C, Ali Z, Sajid M, Akhtar K, et al. Experimental investigation of energy harvesting behind a bluff body. J Renew Sustain Energy 2020;12. https://doi.org/10.1063/1.5144347.
[24] Shi S, New TH, Liu Y. Flapping dynamics of a low aspect-ratio energy-harvesting membrane immersed in a square cylinder wake. Exp Therm Fluid Sci 2013;46:151–61. https://doi.org/10.1016/j.expthermflusci.2012.12.007.
[25] Shi S, New TH, Liu Y. Effects of aspect-ratio on the flapping behaviour of energy-harvesting membrane. Exp Therm Fluid Sci 2014;52:339–46. https://doi.org/10.1016/j.expthermflusci.2013.09.014.
[26] Uddin E, Huang WX, Sung HJ. Actively flapping tandem flexible flags in a viscous flow. J Fluid Mech 2015;780:120–42. https://doi.org/10.1017/jfm.2015.460.
[27] Akaydin HD, Elvin N, Andreopoulos Y. The performance of a self-excited fluidic energy harvester. Smart Mater Struct 2012:21. https://doi.org/10.1088/0964-1726/21/2/025007.
[28] Michelin S, Doaré D. Energy harvesting efficiency of piezoelectric flags in axial flows. J Fluid Mech 2013;714:489–504. https://doi.org/10.1017/jfm.2012.494.
[29] Kim D, Cossé J, Huertas Cerdeira C, Gharib M. Flapping dynamics of an inverted flag. J Fluid Mech 2013;736:1–12. https://doi.org/10.1017/jfm.2013.555.
[30] Kim H, Kang S, Kim D. Dynamics of a flag behind a bluff body. J Fluids Struct 2017;71:1–14. https://doi.org/10.1016/j.jfluidstructs.2017.03.001.
[31] Shan X, Song R, Fan M, Xie T. Energy-harvesting performances of two tandem piezoelectric energy harvesters with cylinders in water. Appl Sci 2016;6:230. https://doi.org/10.3390/app6080230.
[32] Zhang L, Dai H, Abdelkefi A, Wang L. Experimental investigation of aerodynamic energy harvester with different interference cylinder cross-sections. Energy 2019;167:970–81.
[33] Azadeh-Ranjbar V, Elvin N, Andreopoulos Y. Vortex-induced vibration of finite-length circular cylinders with spanwise free-ends: Broadening the lock-in envelope. Phys Fluids 2018:30. https://doi.org/10.1063/1.5042774.
[34] Hu G, Tse KT, Kwok KCS, Song J, Lyu Y. Aerodynamic modification to a circular cylinder to enhance the piezoelectric wind energy harvesting. Appl Phys Lett 2016;109:1–6. https://doi.org/10.1063/1.4967497.
[35] Hu G, Tse KT, Wei M, Naseer R, Abdelkefi A, Kwok KCS. Experimental investigation on the efficiency of circular cylinder-based wind energy harvester with different rod-shaped attachments. Appl Energy 2018;226:682–9. https://doi.org/10.1016/j.apenergy.2018.06.056.
[36] Latif U, Abdullah C, Uddin E, Younis MY, Sajid M, Shah SR, et al. Experimental and numerical investigation of the energy harvesting flexible flag in the wake of a bluff

body. Wind Struct An Int J 2018;26:279–92. https://doi.org/10.1002/9781118713075.
[37] Ding L, Zhang L, Wu C, Mao X, Jiang D. Flow induced motion and energy harvesting of bluff bodies with different cross sections. Energy Convers Manag 2015;91:416–26. https://doi.org/10.1016/j.enconman.2014.12.039.
[38] Derakhshandeh JF, Alam MM. A review of bluff body wakes. Ocean Eng 2019;182:475–88. https://doi.org/10.1016/j.oceaneng.2019.04.093.
[39] Zhang X, Yang W, Zuo M, Tan H, Fan H, Mao Q, et al. An arc-shaped piezoelectric bistable vibration energy harvester: modeling and experiments. Sensors 2018;18:4472. https://doi.org/10.3390/s18124472.
[40] Kwon SD. A T-shaped piezoelectric cantilever for fluid energy harvesting. Appl Phys Lett 2010;97. https://doi.org/10.1063/1.3503609.
[41] Wang J, Zhou S, Zhang Z, Yurchenko D. High-performance piezoelectric wind energy harvester with Y-shaped attachments. Energy Convers Manag 2019;181:645–52. https://doi.org/S0196890418313694.
[42] Liu FR, Zou HX, Zhang WM, Peng ZK, Meng G. Y-type three-blade bluff body for wind energy harvesting. Appl Phys Lett 2018;112:1–6. https://doi.org/10.1063/1.5029415.
[43] Silva-Leon J, Cioncolini A, Nabawy MRA, Revell A, Kennaugh A. Simultaneous wind and solar energy harvesting with inverted flags. Appl Energy 2019;239:846–58. https://doi.org/10.1016/j.apenergy.2019.01.246.
[44] Huertas-Cerdeira C, Fan B, Gharib M. Coupled motion of two side-by-side inverted flags. J Fluids Struct 2018;76:527–35. https://doi.org/10.1016/j.jfluidstructs.2017.11.005.
[45] Tian FB, Luo H, Zhu L, Lu XY. Coupling modes of three filaments in side-by-side arrangement. Phys Fluids 2011;23. https://doi.org/10.1063/1.3659892.
[46] Uddin E, Huang WX, Sung HJ. Interaction modes of multiple flexible flags in a uniform flow. J Fluid Mech 2013;729:563–83. https://doi.org/10.1017/jfm.2013.314.
[47] Jia LB, Yin XZ. Passive oscillations of two tandem flexible filaments in a flowing soap film. Phys Rev Lett 2008;100:1–4. https://doi.org/10.1103/PhysRevLett.100.228104.
[48] Ristroph L, Zhang J. Anomalous hydrodynamic drafting of interacting flapping flags. Phys Rev Lett 2008;101:1–4. https://doi.org/10.1103/PhysRevLett.101.194502.
[49] Xie F, Deng J. A further study of inverted hydrodynamic drafting for flow past two flexible filaments in tandem arrangement. Prog Comput Fluid Dyn 2018;18:164–76. https://doi.org/10.1504/PCFD.2018.091699.
[50] Poole C, Darwazeh I. Introduction; 2016. https://doi.org/10.1016/b978-0-12-407823-9.00001-9.
[51] Uddin E, Huang WX, Sung HJ. Interaction modes of multiple flexible flags in a uniform flow. J Fluid Mech 2013;729:563–83. https://doi.org/10.1017/jfm.2013.314.
[52] Orrego S, Shoele K, Ruas A, Doran K, Caggiano B, Mittal R, et al. Harvesting ambient wind energy with an inverted piezoelectric flag. Appl Energy 2017;194:212–22. https://doi.org/10.1016/j.apenergy.2017.03.016.
[53] Williamson C. Vortex dynamics in the cylinder wake. Annu Rev Fluid Mech 1996;28:477–539. https://doi.org/10.1146/annurev.fluid.28.1.477.
[54] Alben S. Wake-mediated synchronization and drafting in coupled flags. J Fluid Mech 2009;641:489–96. https://doi.org/10.1017/S0022112009992138.
[55] Kim S, Huang WX, Sung HJ. Constructive and destructive interaction modes between two tandem flexible flags in viscous flow. J Fluid Mech 2010;661:511–21. https://doi.org/10.1017/S0022112010003514.
[56] Sultana A, Alam MM, Middya TR, Mandal D. A pyroelectric generator as a self-powered temperature sensor for sustainable thermal energy harvesting from waste heat and human body heat. Appl Energy 2018;221:299–307. https://doi.org/10.1016/j.apenergy.2018.04.003.
[57] Vullers RJM, van Schaijk R, Doms I, Van Hoof C, Mertens R. Micropower energy harvesting. Solid State Electron 2009;53:684–93. https://doi.org/10.1016/j.sse.2008.12.011.
[58] Sauerbrey J, Schmitt-Landsiedel D, Thewes R. A 0.5-V 1-μ W successive approximation ADC. IEEE J Solid-State Circuits 2003;38:1261–5. https://doi.org/10.1109/JSSC.2003.813217.
[59] Moon JW, Jung HJ, Baek KH, Song D, Bin Kim S, Kim JH, et al. Optimal design and application of a piezoelectric energy harvesting system using multiple piezoelectric modules. J Electroceramics 2014;32:396–403. https://doi.org/10.1007/s10832-014-9934-0.
[60] STLM20 - Analog temperature sensor, ultra-low current 2.4 V, high precision - STMicroelectronics n.d. https://www.st.com/en/mems-and-sensors/stlm20.html [accessed September 10, 2020].
[61] IMEC realized world first digital UWB transmitter IC for IEEE 802.15.4a | EE Times n.d. https://www.eetimes.com/imec-realized-world-first-digital-uwb-transmitter-ic-for-ieee-802-15-4a/# [accessed September 10, 2020].